Molecular dynamics simulation of the initial stages of He bubbles formation in silicon

2013 Modelling Simul. Mater. Sci. Eng. 21 065002

(http://iopscience.iop.org/0965-0393/21/6/065002)

Modelling Simul. Mater. Sci. Eng. **21** (2013) 065002 (13pp) doi:10.1088/0965-0393/21/6/065002

Molecular dynamics simulation of the initial stages of He bubbles formation in silicon

L Pizzagalli[1], **M L David**[1] **and M Bertolus**[2]

[1] Department of Physics and Mechanics of Materials, Institut P', CNRS - Université de Poitiers UPR 3346, SP2MI, BP 30179, F-86962 Futuroscope Chasseneuil Cedex, France
[2] CEA, DEN, DEC/SESC/LLCC, Bt. 352, Centre de Cadarache, 13108 Saint-Paul-Lez-Durance, France

E-mail: Laurent.Pizzagalli@univ-poitiers.fr

Received 4 December 2012, in final form 13 June 2013
Published 12 July 2013
Online at stacks.iop.org/MSMSE/21/065002

Abstract

The initial stages of the formation of bubbles due to helium implantation in silicon remain largely unknown, for they occur at time and space scales hardly accessible to experiments. To improve the current knowledge, we have developed an interatomic potential to describe the He : Si system, which can model helium for the pressure conditions expected in bubbles, and reproduce the behaviour of a single helium atom in silicon. Then molecular dynamics calculations were performed. Starting from an initial random distribution of helium interstitials and silicon vacancies, simulations revealed a two-step formation of small He_nV_m clusters. First, available vacancies quickly formed vacancy clusters V_m, due to their high mobility. In a second step, all clusters included a slowly increasing number of helium atoms, which were captured by diffusion or by cluster migration. Migration coalescence coarsening mechanisms were also identified during the simulation.

(Some figures may appear in colour only in the online journal)

1. Introduction

The observation of helium-filled bubbles in silicon following implantation has been routinely reported [1–10]. The extremely low solubility of helium makes bubble formation more favourable than an homogeneous dilution. Such a phenomenon can be beneficial, as the formed bubbles can be emptied and used as traps for metallic impurities [11, 12]. However, it is usually viewed as detrimental since these bubbles are expected to sustend high internal pressures of several GPa [4, 13, 14], which can induce swelling and deterioration of the mechanical properties of the material. This can have dramatic effects in nuclear applications, for which helium-filled bubbles also occur in structural and confinement materials.

In order to be able to inhibit bubble formation, or at least delay it, it is necessary to reach the most complete understanding of the phenomenon, starting from a single helium impurity up to the formation and growth of bubbles. Due to first-principles calculations [15–20] and a few experiments [21, 22], the properties of a single helium atom in silicon, in the presence of or lacking vacancies, have been determined. At the other end of the scale, it is now well established that helium-filled bubbles grow through a mechanism involving bubble migration and coalescence [23, 24]. The uncertainty remains on the intermediate regime, i.e. the first stages of the formation of helium-filled bubbles. In fact, this regime is operating at time and space scales both difficult to attain experimentally, or using first-principles calculations. Possible alternatives include classical molecular dynamics simulations, which should be able to describe the initial formation stages, provided a time scale of the order of a nanosecond is sufficient.

The main obstacle for performing such simulations is the lack of available interatomic potentials for modelling the He : Si system. To the best of our knowledge, only purely repulsive pair potentials have been used in earlier investigations [25, 26]. For reasons which will become clear in the following, these potentials are not suited to describe the interaction between He atoms and vacancies during the first stages of bubble formation. To bypass this issue, we have built a modified embedded atom method (MEAM) [27] potential, which is presented in this work. The potential was validated on a few simple configurations, then used to perform molecular dynamics simulations of the formation of helium bubbles precursors starting from configurations including an initial random distribution of vacancies and helium interstitials.

2. MEAM parametrization

To describe the atomic interactions in the He : Si, the MEAM formalism was selected, since it allows energy and forces calculations in a many-body framework [27]. This could appear as a surprising choice since it is rather customary for helium to consider either (1) a repulsive potential for short range interactions in an irradiation context [25, 26], or (2) a Lennard-Jones or Buckingham potential for an accurate modelling of weak dispersive attractive forces. Ideally, one would combine both aspects in a single potential. The MEAM formalism is flexible enough for this task.

Then, another aspect specific to the He : Si systems, has to be taken into account. All preceding investigations revealed that it is energetically more favourable for a single helium atom to be located in a tetrahedral interstitial site rather than in a vacancy [15–18], with a quite important energy difference. In the cubic diamond structure, the tetrahedral interstitial location is equivalent to a silicon node lattice with respect to first neighbours (four at a distance of $\sqrt{3}a_0/4$). Both locations become inequivalent when considering second neighbours, 12 at a distance of $a_0/\sqrt{2}$ for the silicon node lattice, and 6 at a distance of $a_0/2$ for the tetrahedral site. Given the weak attractive tail of He interactions, a simple pair potential will necessarily yield very similar energies for both locations. Conversely, in addition to a pair interaction, the MEAM potential includes an embedding energy term which depends on the host pseudodensity [27][3]. Due to the angular dependence in the calculation, pseudodensities at the lattice node and tetrahedral site can be made significantly different. Then, a MEAM potential should be a simple and 'physical' way to discriminate between both sites.

[3] The original MEAM formalism has been modified regarding partial electron density in more recent papers (see, for instance, [28]). Note that here we used the original version, as described in [27], which is the current default behaviour in the LAMMPS code.

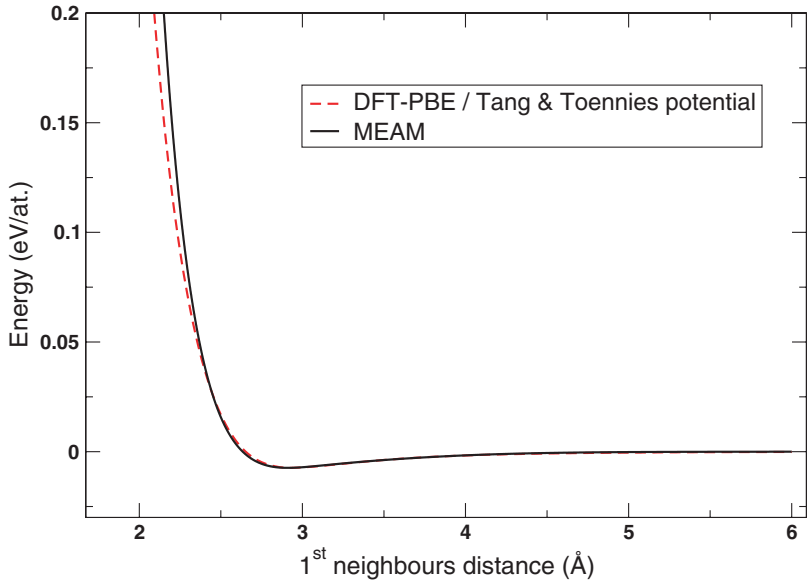

Figure 1. Energy of helium in the hcp phase as a function of first neighbours distance for the MEAM potential developed in this work (full line), and using the Tang and Toennies potential [29] for the attractive part combined with DFT-PBE calculations for the repulsive part (dashed line).

2.1. Fitting procedure

In the MEAM formalism, a reference structure is required for each kind of interatomic interactions. For the He–He interaction, an hcp lattice was considered as helium crystallizes in this structure at low temperature and high pressure [30]. Equation (1) shows the Rose energy function E^r used in our work. This formulation has been employed in recent MEAM parametrizations and is also included in the molecular dynamics code LAMMPS, which is used for numerical simulations in the next section:

$$E^r = -E_c(1 + a_* + a_3(a_*^3)/(r/r_e)) \exp(-a_*), \tag{1}$$

where $a_* = \alpha(r/r_e - 1)$ and a_3 can have two values, depending whether r is greater or lower than r_e. For the reference data needed for the fit, we first considered the attractive part calculated using the pair potential developed by Tang and Toennies [29], which is fitted on high level computations in this regime, since it is known that density functional theory (DFT) calculations poorly reproduced weakly dispersive attractive interactions. The most stable state is obtained for a cohesive energy $E_c = 7.3775$ meV/at. and an equilibrium distance $r_e = 2.9113$ Å. For the repulsive part, we have performed DFT calculations using the Quantum Espresso package [31]. The Perdew–Burke–Ernzerhof (PBE) functional [32] was employed, as recent investigations suggested that it is one of the most accurate exchange correlation functional for helium [33, 34]. In that case, the ground state is characterized by $E_c = 10.796$ meV/at. and $r_e = 2.8995$ Å, in surprisingly good agreement with the above result. The full curve, obtained by combining the two set of results and slightly shifting the DFT-PBE curve, is shown in figure 1.

Our first attempt to fit equation (1) indicated that in order to reproduce both the potential well and the smooth curvature in the repulsive regime, a negative value of a_3 is required for distance lower than r_e. Unfortunately, using a negative value also induces a potentially annoying side effect, since an attractive regime is recovered for short He–He distances. Such

Table 1. MEAM parameters used in this work.

	Si [27]	He	SiHe
Struct.	Diamond	hcp	Dimer
E_c	4.63	0.0073775	0.0077
r_e	5.431	2.9113	2.912
α	4.87	10.5	9.0
A	1.0	−0.35	
$\beta^{(0)}$	4.4	0.75	
$\beta^{(1)}$	5.5	0.0	
$\beta^{(2)}$	5.5	0.0	
$\beta^{(3)}$	5.5	0.0	
$t^{(0)}$	1.0	1.0	
$t^{(1)}$	3.13	1.0	
$t^{(2)}$	4.47	1.0	
$t^{(3)}$	−1.80	1.0	
ρ_0^a	2.35	109.0	
a_3 ($r > r_e$)		0.15	0.011
a_3 ($r < r_e$)		0.0	0.011

a behaviour, in addition to being non-physical, may have dramatic results in simulations involving high kinetic energies (high temperatures, cascades), with a potential risk of two helium atoms collapsing. We therefore set $a_3 = 0.0$ for distances lower than r_e. As a consequence, the fitted curve departs from the reference curve for small He–He distances (figure 1), thus overestimating high pressures. The proposed MEAM helium potential will then not be suited to model helium under very high pressure conditions. Nevertheless, a reasonable agreement is obtained for pressures below 10 GPa, which are the aimed conditions of the current investigation. We also computed the heat of formation and lattice parameters for common crystalline structures. It is found that fcc is slightly less favoured than hcp, and also that other cubic structures such as bcc or simple cubic are associated with much lower heats of formation. These results are in agreement with what one would expect for solid helium, and further assess that the present MEAM helium parametrization is correct.

Since there is no stable silicon–helium compound, we selected a dimer reference structure for the Si–He interaction. Required data were obtained from first-principles calculations, as in the case of He–He parameters. The remaining parameters, A, ρ_0^a, $\beta^{(i)}$ and $t^{(i)}$, were determined by performing a downhill simplex minimization. In the fitting database, we included the formation energies and geometries of all different possible configurations for a single helium atom into silicon bulk, in the presence of or lacking a vacancy [18], which were calculated using DFT-PBE calculations and a $3a_0 \times 3a_0 \times 3a_0$ supercell ($a_0 = 5.468$ Å), a plane wave cutoff of 15 Ry, and a $2 \times 2 \times 2$ Monkhorst-Pack k-point sampling [35]. In addition, we included the pressure associated with different densities for bulk hcp helium according to experiments [30]. During the fitting procedure, we found that for helium the quality of the fit depends only very slightly on high order contribution in the calculation of electron density [27]. Then, ($\beta^{(i)}, t^{(i)}, i = 1$–3) were just set to constant values. Final parameters are shown in table 1.

2.2. Results

Table 2 shows the data used for the fit and the results obtained with the final parametrization of the potential. The energy ordering of the different configurations for a single He in Si is correct,

Table 2. Various properties used in the fit of the Si–He potential proposed in this work. Reference data were obtained using DFT-PBE calculations and a 216-atoms cell for energies (eV), distance (Å), or from experiments [30] for pressure (GPa).

	Reference	Result
Formation energy (He in T)	1.00	1.15
Formation energy (He in H)	1.65	1.85
Formation energy (He in V_1)	1.61	1.60
Formation energy (He 1^{nn} of V_1)	1.16	1.27
Migration energy (T-H-T)	0.65	0.70
Si–He distance (He in T)	2.415	2.387
Si–He distance (He in H)	2.341	2.296
Pressure HCP He (4.3 mol cm^{-3})	1.0	1.15
Pressure HCP He (5.2 mol cm^{-3})	5.0	7.1

with He in the tetrahedral site T favoured over the hexagonal site H and the substitional site (He in a vacancy). Also the energy of one helium atom in a T site first-neighbour to a vacancy is well reproduced. The computed migration energy for the T-H-T path [15] is reproduced with a good accuracy. Finally, the pressure for solid helium at fixed density is slightly overestimated with the potential, as previously explained, but the difference remains small and acceptable.

In order to assess the transferability of the developed potential in simple situations, it was used to compute the best configuration for a few small He_nV_m clusters. To the best of our knowledge, the properties of such clusters are not known, since there are no available calculations or experiments. Then we have performed DFT-PBE calculations, using the same parameters reported above, for He_2V_1, He_2V_2 and He_4V_2. In each case, several initial He positions were tried in order to determine the most stable configuration. Theses results were then compared with those obtained using the potential.

Figure 2 shows the most stable configurations obtained from first-principles calculations. For He_2V_1, the lowest energy state is characterized by the two helium atoms off the vacancy, and forming a short dimer with length 1.90 Å aligned along two T sites. With the Si–He potential, this configuration is also found as the most stable, with a difference in formation energy of only 0.14 eV, albeit with a slightly larger He–He dimer (2.33 Å). The second best geometry corresponds to one helium atoms in the vicinity of the vacancy and the second one close to a T site for both DFT-PBE and the Si–He potential. For He_2V_2, the two helium atoms form a dimer of length 2.26 Å approximately centred on one of the vacancies in DFT-PBE calculations. A higher energy configuration is obtained when each helium atom is located in the vicinity of a vacancy. With the Si–He potential, the most stable configuration is equivalent, although the distance between helium atoms is now 2.69 Å, with a difference in formation energy of 0.23 eV. Finally, the most stable configuration for He_4V_2 is characterized by the formation of a distorted rhombus, similar to the basal plane packing of the hcp lattice and defining a plane roughly perpendicular to the line linking the two vacancy centres (figure 2). This geometry is also obtained as the most stable one using the Si–He potential, with a difference of 0.42 eV for the formation energy, and larger distances between helium atoms.

Overall, we found good agreement between DFT-PBE and the Si–He potential regarding the energies and geometries of these small He_nV_m clusters, which suggests that the potential is suited for investigating the first stages of helium and vacancies aggregation. Nevertheless, it is important to emphasize here that the number of possible configurations grows extremely fast with n and m. We did not try to perform an exhaustive search here and, as a consequence, we do not claim to have found the most stable structures in each case.

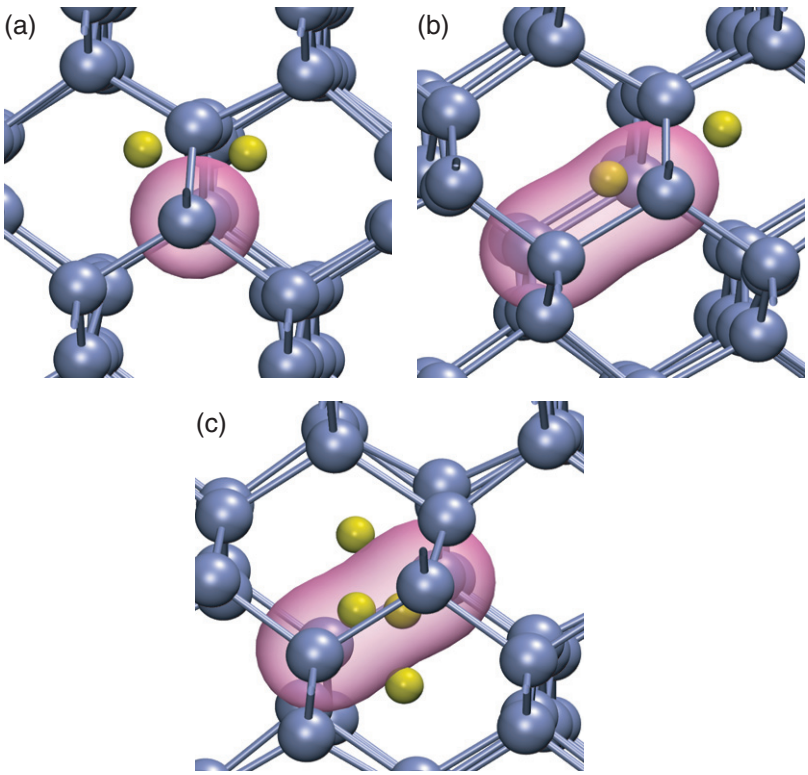

Figure 2. Most stable configurations for He_2V_1 (*a*), He_2V_2 (*b*) and He_4V_2 (*c*), obtained from DFT-PBE calculations. Si (He) atoms are represented by blue (yellow) spheres. The mono- or divacancy region are shown as transparent pink volumes.

3. Mechanisms of He-filled bubbles formation

The Si–He potential described in the previous section was used to perform molecular dynamics simulations of the first stages of He-filled bubbles formation. Important initial data are the helium and vacancy concentrations in the simulation. In the case of helium implantation, both quantities depend on various implantation conditions such as the fluence, the He impinging energy, the temperature and the dose-rate [3–5, 7, 36, 37]. It is known that at low fluence, typically below $1 \times 10^{15}\,\mathrm{cm}^{-2}$, no He-filled defects are observed. For medium fluences, between 1×10^{15} and $5 \times 10^{16}\,\mathrm{cm}^{-2}$, various He-filled defects can be observed, typically bubbles and platelets. Finally, at fluences greater than about $5 \times 10^{16}\,\mathrm{cm}^{-2}$, He-filled bubbles are always observed.

In this work, we have considered a situation corresponding to a standard 100 keV helium implantation with a fluence of $1 \times 10^{16}\,\mathrm{cm}^{-2}$. A SRIM calculation indicates that under these conditions a maximum helium concentration of about $5 \times 10^{20}\,\mathrm{cm}^{-3}$ is reached in silicon [38]. The vacancy concentration is much more difficult to estimate. In fact, SRIM calculations suggest that large concentrations of vacancies could be created during implantation. However, a large proportion should also vanish by recombination, an effect strongly dependent on the implantation temperature and not taken into account in SRIM simulations. Furthermore, knowing the exact nature of the remaining vacancy defects is a real issue. Nevertheless, assuming that only single vacancies remain in the implanted

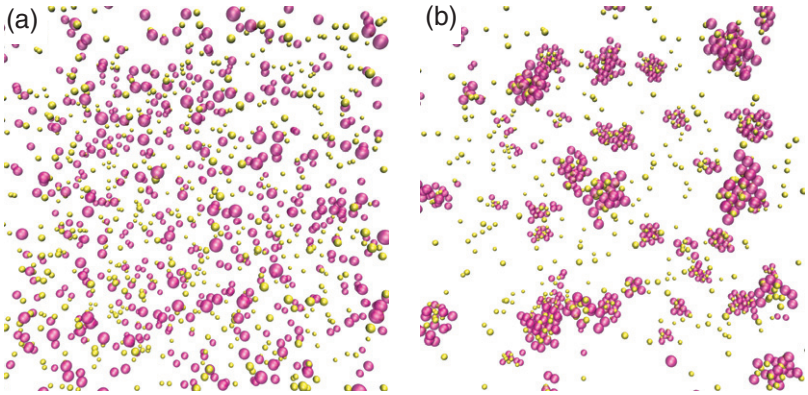

Figure 3. Partial representation of a silicon bulk system including 720 helium atoms and 633 vacancies: (*a*) initial and (*b*) final states, after 10 ns at 1400 K. Only helium atoms (yellow spheres) and vacancies (pink spheres) are shown.

material, positron annihilation spectroscopy experiments revealed an order of magnitude of about 10^{20} cm^{-3} for the concentration [37]. In the following, similar helium and vacancy concentrations will be employed.

3.1. Technical details

The simulations were performed using the LAMMPS code [39], a standard package for classical molecular dynamics calculations. Our system was built as a $20a_0 \times 20a_0 \times 20a_0$ silicon box with $a_0 = 5.431$ Å, in which 633 single vacancies were randomly created. Then, 720 helium atoms were randomly positioned in tetrahedral interstitial sites. These numbers correspond to helium and vacancies concentrations of 5.618×10^{20} cm^{-3} and 4.939×10^{20} cm^{-3}, respectively. Figure 3(*a*) shows the 64 087 atoms system in its initial state. Then, a molecular dynamics calculation in the NVT ensemble was performed during 10 ns (2×10^7 iterations with a 0.5 fs timestep), and with a temperature of 1400 K. Such a high temperature was chosen to allow for an easiest activation of migration mechanisms during the short duration of the simulation, one of the most important shortcomings of molecular dynamics. Note that this is not an unrealistic condition, since it is well known that thermal spikes can occur during the implantation process, inducing very high temperatures that may eventually lead to localized melting.

The state of the system was periodically recorded during the simulations for analysis. The main difficulty for the analysis is the fast characterization of vacancy-like defects at each step. Here, we simply associate each silicon atom in the defected system with the nearest node of the cubic diamond lattice, at time t. This technique, possible only in a crystal, allows for a very fast determination of empty nodes, i.e. the vacancies. Knowing the positions of helium atoms and vacancies, it becomes straightforward to compute the distribution of $\mathrm{He}_n\mathrm{V}_m$ clusters at each t according to a connectivity criterion. We considered that two helium atoms were connected when their separation was less than 3 Å, i.e. approximately between the first and second neighbours distance. For helium atoms and vacancies, it was shown that a noticeable interaction exists only for short separations [18]. Here we considered a maximum distance of 2 Å. Finally, a separation criterion of 4 Å, roughly between the second and third neighbours distances in silicon, was used between two vacancies, since it is known that two mono-vacancies in second neighbours locations already form a bound state [40]. Note that the results and conclusions reported in the next sections remain qualitatively the same even if different distance criteria are used for connectivity determination.

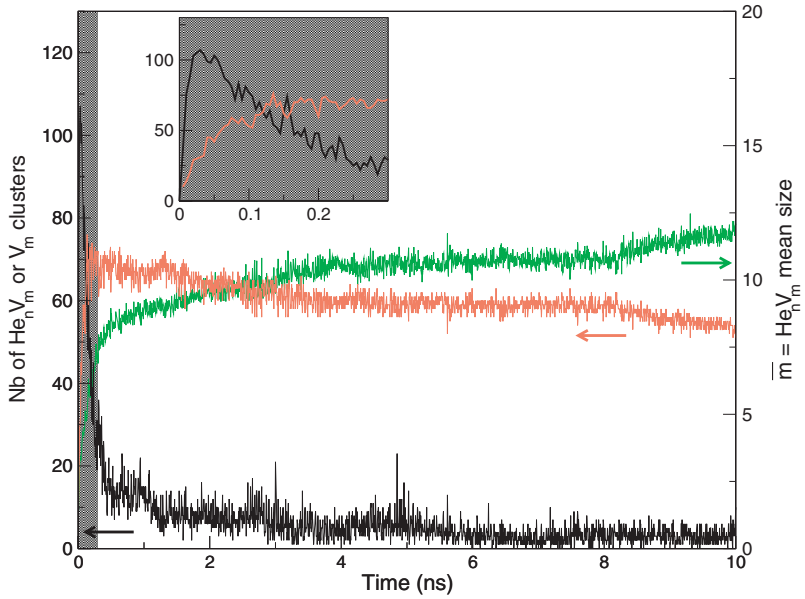

Figure 4. Numbers of He_nV_m (red curve) and V_m (black curve) clusters (left axis), and average size of He_nV_m clusters (green curve, right axis), as a function of time. The inset shows the evolution of the numbers of clusters for the first 300 ps (grey area).

3.2. Results

The initial and final states of the simulation are shown in figure 3. Starting from an homogeneous random distribution of helium interstitials and silicon vacancies, the 10 ns run at 1400 K makes the system evolving towards a new configuration, which includes several He_nV_m clusters of various sizes and a remaining homogeneous distribution of single helium atoms. The connectivity analysis revealed that 50 He_nV_m clusters are present in the final state, with compositions ranging from He_2V_3 to $He_{18}V_{33}$. Only seven clusters with no helium atoms, characterized by small sizes ($m < 8$), remained. Finally, approximately 43% of single helium atoms remain, in agreement with the visual feeling from figure 3.

In order to understand the details of the system evolution, the variation as a function of time of several quantities characterizing He_nV_m clusters were analysed (figures 4 and 5). At the beginning of the annealing, the most striking feature is a very fast increase of the number of V_m vacancy clusters (black line in the inset of figure 4). The maximum number of such clusters is reached after only 50 ps, most of those being V_2, V_3 and V_4. This fast clustering of vacancies is due to several factors. First, it is energetically favourable to aggregate vacancies in silicon [41]. Then, the mobility of the single vacancy is high, the energy barrier for migration being only 0.43 eV with the potential in agreement with the litterature [40]. Finally, another favourable factor is the high initial density of available single vacancies, which strongly reduces their mean free path. These findings are in agreement with previous investigations of vacancy clustering in silicon [42, 43].

After reaching this maximum, the number of V_m decreases quickly, albeit at a lower rate than previously. After 1 ns, less than 10 V_m clusters remained in the system. This variation is correlated with the increase of the number of He_nV_m clusters (red line in figure 4), which reaches a maximum of about 70 after 150 ps. The cause of the decrease of the number of V_n

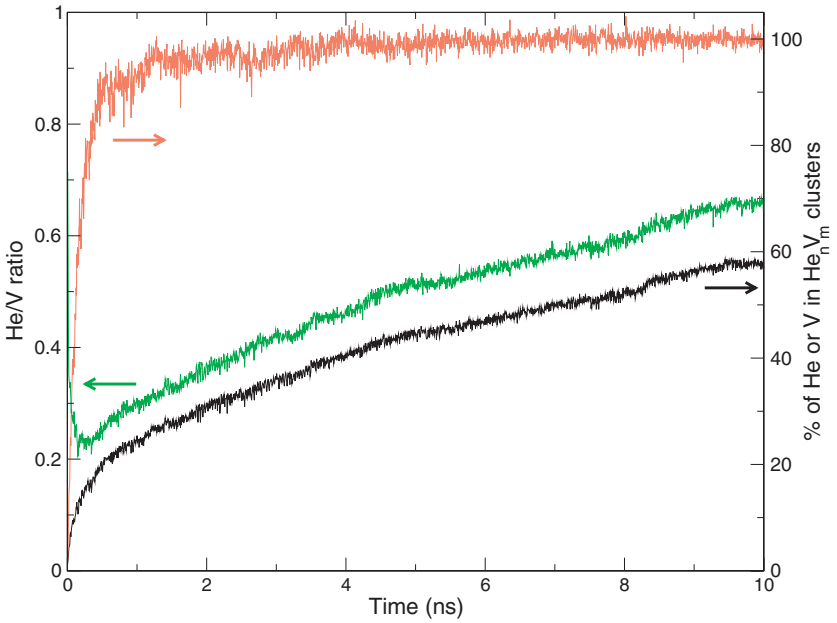

Figure 5. He/V ratio (green curve, left axis), and percentages of helium atoms (black curve) and vacancies (red curve) in He_nV_m clusters (right axis), as a function of time.

is not clustering, but rather the capture of available helium atoms. The lower slope for the increase of the He_nV_m number may be explained by the lower diffusion coefficient of helium, the energy barrier with the potential being 0.70 eV. It is also possible that capture occurred by migration of the V_m clusters. In all cases, the short time scale of the process suggests that He_nV_m form from helium atoms and V_m clusters initially separated by small distances.

Then, from 200 to 500 ps, the mean size of He_nV_m clusters (determined as $\overline{m}$) increases with a rate which tends to decrease over time (figure 4), due to the scarcity of available vacancies. In fact, the analysis of the variation of the percentage of vacancies and helium atoms in He_nV_m clearly shows that only about 10% vacancies remain available (figure 5). Meanwhile, the vast majority of helium atoms are not contained into He_nV_m clusters, but remain as single interstitials. We found that the formation of small He_n clusters can occur during the simulation, but with an extremely short lifetime. This is in agreement with previous investigations showing that the interaction between two helium atoms in silicon is very weak [15].

After approximately 400–500 ps, the first step of He_nV_m formation is achieved. The system is close to the final state, although He_nV_m clusters are more numerous and smaller on average. They also contained fewer helium atoms ($\simeq$20% of the total number), and a minimum value of about 0.23 is obtained for the He/V ratio (figure 5). The second step of He_nV_m formation, from 500 ps until the end of the simulation, is mainly characterized by the slow capture of the remaining available helium atoms by the He_nV_m clusters already formed. This appears clearly in the variation of the numbers of helium atoms in He_nV_m clusters, as well as the associated increase in the He/V ratio (figure 5). Again, this process may occur via the migration of the helium atoms, or of the clusters itself. Our simulations suggest that the former are more mobile than the latter, but additional investigations would be necessary for definitive conclusions.

In addition to the capture of helium atoms, the curves plotted in figure 4 revealed a slow and continuous increase in the mean size of He_nV_m clusters, associated with a decrease of

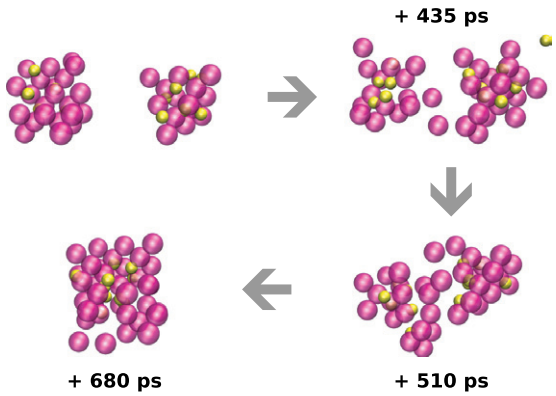

Figure 6. Selected steps of a coalescence mechanism occurring during the molecular dynamics simulation between two He_nV_m clusters (similar colour code to figure 3).

Table 3. Mobility properties for the diffusive species involved in this work.

	Migration energy (eV) at 0 K	Diffusivity ($m^2\ s^{-1}$) at 1400 K
Silicon vacancy	0.43	2.35×10^{-7}
Helium interstitial	0.70	7.37×10^{-9}

their numbers, during this second stage. Two mechanisms have been proposed to explain the coarsening of He_nV_m clusters. Ostwald ripening leads to the exhaustion of small clusters by the loss of vacancies in favour of the bigger ones. The second mechanism involves migration and coalescence of the clusters. We observed occurrences of the latter in our simulation. For instance, figure 6 shows the subsequent steps leading to the formation of a $He_{13}V_{36}$ cluster by the coalescence of He_6V_{14} and He_6V_{22} (an additional single helium atom is captured during the process). Although a precise identification of the initial and final states of the mechanism is rather subjective, the total duration of the process is about 700 ps. The analysis we have performed so far did not allow us to prove that Ostwald ripening processes occurred during the run, but this possibility cannot be excluded. Additional investigations and a deeper analysis, beyond the scope of this work, are obviously required.

Then it can be concluded that the formation of large He_nV_m clusters is a two-step process, with the aggregation of highly mobile vacancies first. The second step consists in the evolution of these seeds through coarsening events and filling by the slower helium atoms. Such a result is the consequence of the difference in mobility between silicon vacancies and helium interstitials. In fact, the 0 K computed migration energies for both species are 0.43 eV and 0.7 eV, respectively (see table 3). We have also evaluated the diffusivity at 1400 K from the computation of the average time between two migration events in our simulations. The results, reported in table 3, indicate that the vacancy is about 32 times more mobile than the helium interstitial at this temperature.

Finally, it clearly appears that the evolution of the He_nV_m clusters is not complete after our 10 ns molecular dynamics simulation. There are still 43% of available helium atoms into the system. Their capture by the He_nV_m clusters would allow the system to overcome the He/V ratio maximum value of 0.66 that is reached at the end of the simulation. Also, while the formed He_nV_m clusters can probably be qualified as precursors of the experimentally observed bubbles, their size remain far from the latter. In fact, considering that a vacancy represents

the same volume than a bulk silicon atom, we found that after 10 ns the average cluster size is equivalent to a bubble of a diameter of 0.8 nm, and the largest cluster to a bubble of a diameter of 1.1 nm. Such bubbles can be considered as the precursors of experimentally observed larger bubbles.

4. Conclusion

In this work, we have developed a silicon–helium potential using the MEAM formalism, which allows for the correct energetic ordering of the possible configurations of a single helium atom in silicon. This potential is best suited to describe helium for pressures lower than 10 GPa. It has been validated in the case of small He_nV_m aggregates, by comparison with first-principles calculations.

The potential was used to perform a long molecular dynamics simulation (10 ns) starting from a random distribution of helium interstitials and silicon vacancies, which revealed two well-defined steps in the formation of large He_nV_m clusters. In the first one, available vacancies quickly formed vacancy clusters V_m, due to their high mobility. These defects can include few helium atoms, which were initially close to the vacancy aggregates and then easily captured. In a second step, all clusters included a slowly increasing number of helium atoms, which were captured by diffusion or by cluster migration. In addition, a coarsening of the He_nV_m distribution was observed, with a slow increase in the average cluster size and a decrease of their number. A mechanism of migration and coalescence was identified as one of the cause for this coarsening. However, other mechanisms such as Ostwald ripening cannot be excluded.

The classical molecular dynamics results presented in this work are a good example of the new perspectives offered by this potential. Although the time scale limitation of molecular dynamics prevents the investigation of the formation of large bubbles starting from individual particles, a large list of exciting situations can now be addressed. Possible examples are the influence of helium density on the stability and mobility of He_nV_m clusters, the effect of temperature, or the investigation of the Ostwald ripening process using a model system.

Acknowledgments

Professor Kai Nordlund is gratefully acknowledged for providing a Si–He pair potential that was used for initial tests.

References

[1] Griffioen C C, Evans J H, De Jong P C and van Veen A 1987 Helium desorption/permeation from bubbles in silicon: a novel method of void production *Nucl. Instrum. Methods Phys. Res.* B **27** 417

[2] Fichtner P F P *et al* 1998 Nucleation and growth of platelet bubble structures in He implanted silicon *Nucl. Instrum. Methods Phys. Res.* B **136–138** 460

[3] Fichtner P F P, Kaschny J R, Behar M, Yankov R A, Mücklich A and Skorupa W 1999 The effects of the annealing temperature on the formation of helium-filled structures in silicon *Nucl. Instrum. Methods Phys. Res.* B **148** 329

[4] Raineri V, Coffa S, Saggio M, Frisina F and Rimini E 1999 Radiation damage–He interaction in He implanted Si during bubble formation and their evolution in voids *Nucl. Instrum. Methods Phys. Res.* B **147** 292

[5] Beaufort M-F, Oliviero E, Garem H, Godey S, Ntsoenzok E, Blanchard C and Barbot J-F 2000 Defects in silicon induced by high energy helium implantation and their evolution during anneals *Phil. Mag.* B **80** 1975

[6] Oliviero E, David M-L, Beaufort M-F, Barbot J-F and van Veen A 2002 On the effects of implantation temperature in helium implanted silicon *Appl. Phys. Lett.* **81** 4201

[7] David M-L, Beaufort M-F and Barbot J-F 2003 Effect of implant temperature on defects created using high fluence of helium in silicon *J. Appl. Phys.* **93** 1438
[8] Frabboni S, Corni F, Nobili C, Tonini R and Ottaviani G 2004 Nanovoid formation in helium-implanted single-crystal silicon studied by *in situ* techniques *Phys. Rev.* B **69** 165209
[9] Maekawa M and Kawasuso A 2010 Characterization of helium bubbles in Si by slow positron beam *J. Phys. Conf. Ser.* **225** 012032
[10] Raineri V, Saggio M and Rimini E 2000 Voids in silicon by He implantation: from basic to applications *J. Mater. Res.* **15** 1449
[11] Raineri V, Battaglia A and Rimini E 1995 Gettering of metals by He induced voids in silicon *Nucl. Instrum. Methods Phys. Res.* B **96** 249
[12] Follstaedt D M, Myers S M, Petersen G A and Medernach J W 1996 Cavity formation and impurity gettering in He-implanted Si *J. Electron. Mater.* **25** 157
[13] Hueging N, Luysberg M, Trinkaus H, Tillmann K and Urban K 2006 Quantitative pressure and strain field analysis of helium precipitates in silicon *J. Mater. Sci.* **41** 4454
[14] David M-L, Pailloux F, Mauchamp V and Pizzagalli L 2011 *In situ* probing of helium desorption from individual nanobubbles under electron irradiation *Appl. Phys. Lett.* **98** 171903
[15] Alatalo M, Puska M J and Nieminem R M 1992 First-principles study of He in Si *Phys. Rev.* B **46** 12806
[16] Estreicher S K, Weber J, Derecskei-Kovacs A and Marynick D S 1997 Noble-gas-related defects in Si and the origin of the 1018 meV photoluminescence line *Phys. Rev.* B **55** 5037
[17] Zavodinsky V G, Gnidenko A A, Misiuk A and Bak-Misiuk J 2005 *Ab initio* simulation of high pressure influence on He–H interaction in silicon *Vacuum* **78** 247
[18] Charaf Eddin A, Lucas G, Beaufort M F and Pizzagalli L 2009 DFT calculation of the stability and mobility of noble gas atoms in silicon *Comput. Mater. Sci.* **44** 1030
[19] Charaf Eddin A 2011 Theoretical study of the stability and the mobility of noble gas atoms in silicon and silicon carbide *PhD Thesis* Université de Poitiers
[20] Charaf Eddin A and Pizzagalli L 2012 First-principles calculations of helium and neon desorption from cavities in silicon *J. Phys.: Condens. Matter* **24** 175006
[21] van Wieringen A and Warmoltz N 1956 On the permeation of hydrogen and helium in single crystal silicon and germanium at elevated temperatures *Physica* **22** 849
[22] Jung P 1994 Diffusion of implanted helium in Si and SiO_2 *Nucl. Instrum. Methods Phys. Res.* B **91** 362
[23] Evans J H 2002 Mechanisms of void coarsening in helium implanted silicon *Nucl. Instrum. Methods Phys. Res.* B **196** 125–34
[24] Donnelly S 2006 Some solved and unsolved problems in transmission electron microscopy studies of radiation damage in solids *Ion Beam Science: Solved and Unsolved Problems. Invited Lectures Presented at a Symp. Arranged by the Royal Danish Academy of Sciences and Letters (Copenhagen, Denmark)* vol 1, ed P Sigmund, p 329
[25] Okuniewski M A, Ashkenazy Y, Heuser B J and Averback R S 2004 Molecular dynamics suimulations of void and helium bubble stability in amorphous silicon during heavy-ion bombardment *J. Appl. Phys.* **96** 4181
[26] Nordlund K private communication
[27] Baskes M I 1992 Modified embedded-atom potentials for cubic materials and impurities *Phys. Rev.* B **46** 2727
[28] Baskes M I 1999 Atomistic potentials for the molybdenum–silicon system *Mater. Sci. Eng.* A **261** 165
[29] Tang K T and Toennies J P 2003 The van der waals potentials between all the rare gas atoms from He to Rn *J. Chem. Phys.* **118** 4976
[30] Loubeyre P, LeToullec R, Pinceaux J P, Mao H K, Hu J and Hemley R J 1993 Equation of state and phase diagram of solid ^{4}He from single-crystal x-ray diffraction over a large p–t domain *Phys. Rev. Lett.* **71** 2272
[31] Giannozzi P *et al* 2009 Quantum espresso: a modular and open-source software project for quantum simulations of materials *J. Phys.: Condens. Matter* **21** 395502
[32] Perdew J P, Burke K and Ernzerhof M 1996 Generalized gradient approximation made simple *Phys. Rev. Lett.* **77** 3865
[33] Patton D C and Pederson M R 1997 Application of the generalized-gradient approximation to rare-gas dimers *Phys. Rev.* A **56** R2495
[34] Bertolus M, Major M and Brenner V 2012 Assessment of density functional theory for bonds formed between rare gases and open-shell atoms: a computational study of small molecules containing He, Ar, Kr and Xe *Phys. Chem. Chem. Phys.* **14** 553
[35] Monkhorst H J and Pack J D 1976 Special points for Brillouin-zone integrations *Phys. Rev.* B **13** 5188
[36] Corni F *et al* 1999 Helium-implanted silicon: a study of bubble precursors *J. Appl. Phys.* **85** 1401

[37] Cerofolini G F, Corni F, Frabboni S, Nobili C, Ottaviani G and Tonini R 2000 Hydrogen and helium bubbles in silicon *Mater. Sci. Eng. Rep.* **27** 1
[38] Ziegler J F, Ziegler M D and Biersack J P 2010 SRIM—the stopping and range of ions in matter *Nucl. Instrum. Methods Phys. Res.* B **268** 1818–23
[39] http://lammps.sandia.gov
[40] Caliste D and Pochet P 2006 Vacancy-assisted diffusion in silicon: A three-temperature-regime model *Phys. Rev. Lett.* **97** 135901
[41] Hastings J L, Estreicher S K and Fedders P A 1997 Vacancy aggregates in silicon *Phys. Rev.* B **56** 10215
[42] Prasad M and Sinno T 2003 Internally consistent approach for modeling solid-state aggregation: I. Atomistic calculations of vacancy clustering in silicon *Phys. Rev.* B **68** 045206
[43] Haley B P, Beardmore K M and Grønbech-Jensen N 2006 Vacancy clustering and diffusion in silicon: kinetic lattice Monte Carlo simulations *Phys. Rev.* B **74** 045217